Sequential binding of zinc triggers tau aggregation

Romain La Rocca[1], Philipp O. Tsvetkov[1,2*], Andrey V. Golovin[3,4,5], Géraldine Ferracci[2], Diane Allegro[1], Pascale Barbier[1], Soazig Malesinski[1], Françoise Guerlesquin[6], François Devred[1,2*].

[1]Aix Marseille Univ, CNRS, UMR 7051, INP, Inst Neurophysiopathol, Fac Médecine, Marseille, France;

[2]Aix Marseille Univ, CNRS, PINT, Plateforme INteractome Timone, Fac Médecine, Marseille, France;

[3]Bioengineering and Bioinformatics Department, M. V. Lomonosov Moscow State University, Leninskie Gory 1, 119992 Moscow, Russian Federation;

[4] Institute of Molecular Medicine, I.M. Sechenov First Moscow State Medical University, Trubetskaya Str. 8, Moscow, 119992, Russia;

[5] National Research University HSE, Myasnitskaya Str. 20, Moscow, 101000, Russia;

[6] Aix-Marseille Univ, CNRS, UMR 7255, Laboratoire d'Ingénierie des Systèmes Macromoléculaires, Institut de Microbiologie de la Méditerranée, Marseille, France.

* Corresponding authors: francois.devred@univ-amu.fr ; philipp.tsvetkov@univ-amu.fr

Authors e-mail: RLR: romain.la-rocca@univ-amu.fr; POT: philipp.tsvetkov@univ-amu.fr; AVG: golovin.andrey@gmail.com; GF: geraldine.ferracci@univ-amu.fr; DA : diane.allegro@univ-amu.fr; PB: pascale.barbier@univ-amu.fr; SM : soazig.malesinksi@univ-amu.fr; FG: guerlesquin@imm.cnrs.fr; FD: francois.devred@univ-amu.fr

Abstract:

Tau protein has been extensively studied due to its key roles in microtubular cytoskeleton regulation and in the formation of aggregates found in some neurodegenerative diseases. Recently it has been shown that zinc is able to induce tau aggregation by interacting with several binding sites. However, precise location of these sites and the molecular mechanism of zinc-induced aggregation remain unknown. Here we used Isothermal Titration Calorimetry (ITC) and Nuclear Magnetic Resonance (NMR) to identify zinc binding sites on hTau40 isoform. These experiments revealed three distinct zinc binding sites on tau, located in the N-terminal part (H14, H32, H94, and H121), the repeat region (H299, C322, H329 and H330) and the C-terminal part (H362, H374, H388 and H407). We then demonstrated that one zinc ion binds first to the repeat region, thus allowing the binding of a second zinc ion to the C-terminal part, while the N-terminal site is independant. Using molecular simulations, we modeled the structure of each site in complex with zinc. Finally, using turbidity and Dynamic Light Scattering (DLS) assays, we showed that the C-terminal site (in particular H388 and H407) is critical for zinc-induced aggregation of tau. Our study highlights key residues involved in zinc induced aggregation of tau. Given the clinical importance of tau aggregation, our findings pave the way for designing potential therapies for tauopathies. Based on our results, we propose a model of zinc-induced aggregation of tau, allowing a better understanding of both the physiological and pathological processes associated with tau-zinc interaction.

Keywords: Tau aggregation, zinc, binding sites, NMR, calorimetry

Introduction

Microtubule-associated protein tau plays a central role in cytoskeleton dynamicity via its regulatory activity on microtubule dynamics, which impacts microtubule functions in various processes such as cell division and axonal stability in neurons [1,2]. Tau has also been shown to be associated with a number of neurodegenerative diseases such as Alzheimer's disease (AD), Parkinson's disease (PD) and frontotemporal lobar degeneration [3–6]. In these Tauopathies, tau forms neurofibrillary tangles, which consist of stacked paired helical filaments (PHF) of hyper-phosphorylated tau molecules [7].

Among the endogenous factors that have been shown to favor tau aggregation, zinc seems to play an important role in AD (see [8] for review), similarly to its role in aggregation of other proteins implicated in neurodegeneration. Indeed, zinc has been identified as a factor favoring the aggregation of amyloid-β [9,10], FUS/TLS [11], TDP-43 [12,13] and tau [14]. Zinc has been shown to increase the toxicity of tau in cells [15] mainly through an interaction with tau. More recently, this effect was confirmed in neurons where zinc induces cell death through the acceleration of tau aggregation [16,17]. Several molecular works proved that zinc can also accelerate aggregation of purified tau constructs [14,18,19], thus confirming the direct effect of zinc on tau. In addition, zinc has been recently shown to induce the formation of reversible aggregation of tau [20,21], and to promote Liquid-Liquid Phase Separation (LLPS) of tau [22,23] which could either be part of the early stages of pathological aggregation similarly to tau phosphorylation[24], or a physiological concurrent pathway.

Despite the importance of zinc binding to tau, the exact binding sites are not currently known. Two reports have already addressed this question and spotted seven residues located in the R2-R3 repeat region of tau (C291, C322, H268, H299, H329, H330, and H362) [14,16]. Among these amino acids, the cysteines located in the repeat region of tau (C291 and C322) were

identified as the core of the interaction between a tau peptide (244-372) and zinc (Figure 1). Two other studies highlighted the binding of zinc in the repeat region using the R3 repeat only [17] and a tau construct lacking the R2 repeat [18]. Two other recent studies conducted by Isothermal Titration Calorimetry (ITC) and mass spectrometry suggested presence of additional lower-affinity sites on tau [19,20]. We have recently proposed these lower-affinity sites to be responsible for the self-assembly of tau [20]. However, the exact nature and location of these elusive sites remained unknown preventing understanding of zinc impact on tau functions and aggregation.

In this work we used a combination of Nuclear Magnetic Resonance (NMR), ITC, turbidimetry and Dynamic Light Scattering (DLS) assays to identify and characterize the zinc binding sites on tau protein. We pinpoint the zinc-binding residues in the high affinity binding site in the R2R3 region and uncover the existence of two novel lower affinity binding sites in N and C terminal parts of tau. We also provide insights into the sequential mechanism of zinc binding to tau and reveal the importance of the C-terminal binding site in tau aggregation.

Methods

Peptide synthesis: Synthetic pR2R3 peptide was purchased from GeneCust.

Protein expression and purification: The full-length tau and histidine mutants were expressed from a pET-3d vector introduced into Escherichia coli BL21(DE3). After 3 h of induction with 0.5 mM isopropyl β-D-1-thiogalactopyranoside (IPTG), cells were centrifuged and the pellets were resuspended into a lysis buffer as previously described. Lysis was pursued using three runs of French press at 4 tones, and non-thermostable proteins were precipitated at 95°C for 11 minutes. Then, the lysate was centrifuged at 30 000 g for 30 min at 4°C, and the supernatant

was injected onto a HiTrap SP Sepharose HP cation exchange column pre-equilibrated with a 50 mM MES pH 6.5 buffer. Tau was eluted with a 50 mM MES NaCl 0.5 M pH 6.5 buffer at 1 mL/min, dialysed three times against 2 L of water at 4°C for 2 h, and dry-lyophilized. For ^{15}N labeled-tau, cells were grown on LB medium, centrifuged and the pellet was solubilized in M9 medium containing ^{15}N ammonium chloride. Prior to use, each tau sample was airfuged at 25 psi and dosed at 280 nm with an extinction coefficient of 7700 $M^{-1}.cm^{-1}$ by spectrophotometry as previously described.

Isothermal Titration Calorimetry: Binding of zinc to tau was analyzed by ITC using a MicroCal iTC200 instrument at 10°C in a 50 mM Tris buffer, in the presence of 1 mM TCEP, pH 7.5. Tau concentrations in the calorimetric cell were 50 µM, whereas zinc concentration was 1 mM in the syringe. Data were analyzed as previously described using the MicroCal Origin software and were fitted with a “one-set-of-sites” for tau-HA, while tau-WT required a “sequential-binding-sites” analysis (number of sites fixed as 2).

Turbidity assays: Zinc-induced self-assembly of tau was monitored with NanoTemper Prometheus NT.Plex instrument equipped with an turbidity module at 350 nm as previously described, using high-sensitivity capillaries. Each capillary contained 30 µM of tau and 120 µM of zinc, except for the control samples which contain only 30 µM of tau. Excitation power was set at 60%, and samples were heated from 15°C to 40°C at 1°C/min. All of the turbidity assays were conducted three independent times individually.

Dynamic Light Scattering: The self-assembly of tau induced by zinc was monitored using Zetasizer Nano ZS from Malvern Instruments as previously described. The cuvette contained 50 µL of 30 µM of tau with or without 120 µM of zinc in a 50 mM Tris buffer, in the presence of 1

mM TCEP, pH 7.5. For each tau construct, three recordings were performed at 40°C, consisting in 10 - 15 runs for each assay.

NMR spectroscopy: NMR spectra were recorded on a Bruker spectrometer 600 MHz equipped with a TCI cryoprobe (Triple Resonance Probe). NMR experiments (^{15}N-HSQC) were performed at 280°K (7°C) on 50 µM for ^{15}N-labeled tau samples and 1 mM for pR2R3 peptide. For the pH variations experiments, tau was resuspended into a sodium phosphate buffer at pH 6.1 and 6.7 respectively. For zinc titrations, the buffer was 20 mM MES, 100 mM NaCl, pH 6.5. Using previous chemical shift assignments, we identified the cross-peaks corresponding to the N-terminal and C-terminal extremities in the full-length tau (BMRB entry 17920) and repeat region in the pR2R3 spectrum (BMRB entry 19253[25]). H362, H374, H388 and H407 were assigned on the tau-WT spectrum by using mutants of tau. Data was processed and analyzed with TopSpin software from Bruker.

Molecular simulations: The Rosetta *de novo* structure prediction method with Monte-Carlo approach was utilized for structure prediction for tau fragments with zinc coordination restraints. Fragment library was built with Robetta web server for the whole tau protein isoform htau40 (UniProt identifier : P10636-8). This fragment library was adopted to three selected regions of tau. Simulations were started from an extended chain and then subjected to *ab initio* folding protocol with zinc coordination restraints with scoring function ref2015. Zinc incorporation was done as it was described in the original report with distance and angle restraints to supposed coordination sphere. All backbone and sidechain torsions and zinc rigid-body degrees of freedom were optimized simultaneously in the all-atom refinement stage according to the original report[26]. For each of three Tau regions, 45,000 models were generated and the first 100 models were selected for further analysis. The top model was chosen based on the pair score.

Surface Plasmon Resonance: SPR experiments were carried out at 15 °C in a Biacore T200 instrument (Cytiva) using the CMD500m sensor chip (Xantec, Dusseldorf, Germany). Tau-WT, tau-HA or tau-LA were amine coupled in separate flow cells at pH 5.5, according to manufacturer's instruction and using 10 mM HEPES/NaOH pH 7.4, 150 mM NaCl, 0.05% Tween 20 as running buffer. Due to the low MW of $ZnCl_2$ and $CaCl_2$ ions in comparison to MW of tau proteins, high density levels of proteins were immobilized on the sensor chip (approximatively 4000 - 8000 RU that corresponds to 87 - 175 fmol/mm^2). A control flow cell without protein was used as reference to subtract unspecific binding of ions to the chip surface. The four flow cells were connected and the running buffer was exchanged with 50 mM Tris, 1 mM TCEP, pH 7.5. $ZnCl_2$ and $CaCl_2$ ions were serially diluted in the running buffer (0.3 - 160 µM) and injected 2 min at 30 µL/min over experimental and reference flow cells. Blank run injections of running buffer were performed in the same conditions. Double-subtracted sensorgrams were used to determine the equilibrium response expressed in RU (Resonance Units), for each concentration. Complete and spontaneous dissociation allowed analysis without regeneration. The K_D value for $ZnCl_2$ ions to the immobilised tau protein were calculated by plotting saturation binding curves using BiaEvaluation software version 2.0 (Cytiva).

Results

Localization of zinc-binding sites

Many studies have concluded that the amino acids responsible for zinc binding to tau are located in the R2R3 repeat region of tau [14,15,17,18]. More recently it was suggested that additional sites would exist most likely located outside of this repeat region [19,20]. In order to identify the zinc binding sites on tau protein, we performed ^{15}N-Heteronuclear Single Quantum Coherence (HSQC) NMR on tau first in the absence, and then in the presence of zinc. Since the amino acid

assignment is not complete for full length tau [27], based on the existing attributions, we conducted two separate sets of NMR experiments, first on the peptide pR2R3, to identify the amino acids implicated in zinc binding in the repeat region, and second on full-length tau, to identify the amino acids implicated in zinc binding outside of the repeat region (see Figure S1).

Identification of zinc binding residues in R2R3 region of tau

To first explore the R2R3 repeat domain of tau, we recorded the ^{15}N-HSQC spectrum at ^{15}N-natural abundance on pR2R3 peptide (pR2R3, Figure 1) in the absence of zinc (Figure 2A, orange peaks). Using the assignment already published for this region (Biological Magnetic Resonance Bank (BMRB entry 19253, [25]), we identified cross-peaks corresponding to all Cys and His residues in this region (C291, H299, C322, H329 and H330). It should be noted that the cross-peak corresponding to C291 was split, suggesting the existence of two possible conformations for this residue.

In the presence of zinc (Fig 2A, blue peaks), only the cross-peaks corresponding to H299, C322, H329 and H330 were shifted, indicating that these four residues of the R2R3 region bind zinc. Interestingly, the addition of zinc only slightly influenced the splitting of C291 cross peak thus possibly favoring one of the two conformations, but not contributing to zinc binding.

Identification of zinc binding residues in N- and C-terminal regions of tau

To explore the N- and C-terminal regions of tau, first we recorded the ^{15}N-HSQC spectrum of full-length tau (Figure 1, tau-WT, wild type) in the absence of zinc (Figure 2B, orange peaks). Using the previously published amino-acid assignment map (BMRB, entry 17920, [27]), we identified the cross-peaks corresponding to H14, H32, H94 and H121 in the N-terminal region. Since none of the four C-terminal histidines were assigned in this map, we generated single

amino-acids mutants for each of the four histidines of this region (Figure 1, tau-H362A, tau-H374A, tau-H388A, and tau-H407A) and recorded ^{15}N-HSQC spectra of these mutants (see Figure S2, orange peaks). This enabled us to identify the cross-peaks corresponding to H362, H374, H388 and H407 on the full-length tau spectrum (Figure 2B, orange peaks).

In order to confirm that all the cross peaks we identified as histidines in the N-terminal region are indeed histidines, ^{15}N-HSQC spectrum of full-length tau was recorded at two different pH (pH 6.1 and pH 6.7) to bring the pH closer to the pKa of histidine. Indeed the cross-peaks corresponding to putative histidine shifted between the two conditions (Figure 2C, green and red peaks).

Having now identified all the histidines in the C-terminal and N-Terminal regions, we performed NMR on full-length tau in the presence of zinc (Figure 2B, blue peaks). The addition of zinc induced a shift of cross-peaks of H14, H32, H94, H121, H362, H374, H388 and H407, which indicated that these residues participate in the chelation of zinc. As expected, cross-peaks corresponding to amino-acids in the proximity of these histidines were also shifted (see Figure S3). Considering the localization of the histidines we identified, our results let us hypothesize the existence of two additional binding sites : one binding site in C-terminal (H362, H374, H388 and H407) and one binding site in N-terminal (H14, H32, H94, H121)

Zinc binding sites in N- and C-terminal regions are independent

In order to demonstrate that the eight identified histidines form two separate independent sites at the N-terminal and in C-terminal of tau, we performed NMR on tau with one of its C-terminal His mutated into Ala (Figure 1, tau-H374A) in the presence of zinc (Figure 2D). Upon mutating this amino acid, the cross peaks corresponding to the other three histidine residues located at

the C-terminus did not shift anymore after adding zinc indicating a loss of zinc binding. Furthermore, this mutation in the C-terminal did not have any impact on zinc-dependent shifting of the cross-peaks corresponding to the histidines in the N-terminal region (H14, H32, H94 and H121). This indicated the existence of two independent zinc binding sites, one in the C-terminal and one in the N-terminal region.

In summary, NMR experiments revealed the presence of three zinc-binding sites in tau, involving histidine and cysteine residues, with one site located in the R2R3 region, and two sites in the N-terminal and in the C-terminal region, independent of each other.

Modelisation of zinc binding sites of tau

NMR data allowed us to modelize the three sites identified in our study with a molecular simulation using three small tau peptides encompassing each zinc binding site. N-terminal site was modelized using Tau peptide (13-122) (Figure 3A), R2R3 site was modelized using Tau peptide (298-331) (Figure 3B), and the C-terminal site was modelized using Tau peptide (361-408) (Figure 3C). In all three cases molecular modelisation revealed that the presence of zinc induced a more condensed conformation of tau by bringing together amino acids that would otherwise be distant. This compaction may result in a more globular shape of tau, which is in agreement with previous published DLS data [20].

Sequential binding of zinc to tau

To investigate the thermodynamics of zinc binding to tau protein we studied its interaction with wild type tau and its mutants using isothermal titration calorimetry at 10°C (Figure 4). The obtained data could be fitted by two models : a two-sets-of-sites model with an overall stoichiometry of 3 and a sequential-binding model with stoichiometry of 2 (Table 1). With the

two-sets-of-sites model, we obtained one high affinity binding site (K_a = 2.1±0.7x10^6) and two low affinity ones (K_a = 5.0±1.6x10^4), while with the sequential-binding model we obtained one high affinity binding site (K_a = 1.3±0.2x10^6) and one low affinity site (K_a = 2.7±0.3x10^4). In both models, there was a high-affinity site with a favorable enthalpy and an unfavorable entropy, while the low-affinity site(s) are both enthalpy and entropy favorable (Table 1). Two-sites sequential binding model fitted well, while NMR data revealed three binding sites. This would not be contradictory with the fact we found three sites by NMR, if one of the low affinity sites has a ΔH close to zero and thus is not visible by ITC.

Since ITC of tau-WT did not allow us to distinguish between the 2 models, we used two mutants of tau : one missing all eight zinc binding residues in C- and N- terminal regions (Figure 1, tau-HA, high affinity) and one missing all four zinc binding in the R2R3 region (Figure 1, tau-LA, low affinity). ITC of zinc binding to tau-HA (Figure 4, orange curve) resulted in a calorimetric curve that could now be fitted directly with a one-set-of-site model with stoichiometry (N) of 0.8±0.1, an affinity constant (K_a) of 1.7±0.2x10^5 M^{-1}, an enthalpy (ΔH) of -7.4±0.3 kcal/mol and an entropy (ΔS) of -2.31 cal/mol/deg (Table 1). Thus, the absence of low-affinity zinc binding sites in this mutant indicated that the high affinity site was located in the R2R3 region, which is consistent with previously published data [14,16–18]. Furthermore, ITC titration by zinc of tau-LA in which all cysteines and histidines located in the R2R3 region are mutated (Figure 1, tau-LA) was not accompanied by any heat exchange (Figure 4, brown curve), which indicated that no zinc binding to tau can be detected by ITC in the absence of prior zinc binding in the R2R3 region of tau. These results are consistent only with a sequential binding model where zinc binding to the R2R3 high affinity site induces the formation of a low affinity site while the third site is not “visible” for ITC. Interestingly, using Surface Plasmon Resonance [SPR] we were able to measure zinc binding to one low affinity binding site on WT-tau (see Figure S4) pointing to

significant conformational changes upon this binding. The absence of SPR signal with tau-LA and tau-HA mutants enabled us to conclude that the site evidenced by SPR on WT-tau is the low affinity site induced by the prior binding of zinc to R2R3 high affinity site.

Tau aggregation is triggered by zinc binding to C-terminal low affinity site

Recently it was shown that zinc induces temperature-dependent reversible aggregation of tau [20]. To understand the role of each zinc binding site in this process, we used turbidimetry assays to follow aggregation of WT tau and its mutants as previously described [20]. The sample containing tau-WT and zinc was heated from 15°C to 40°C while measuring the turbidity at 350 nm (Figure 5A, blue curve). In these conditions, the turbidity increased at 20°C, indicating that zinc was able to trigger the temperature reversible aggregation of tau described recently [20]. DLS experiments revealed the absence of the monomeric peak with the formation of particles that are out of the range of DLS detection (see Figure S5A, blue curve), and a slow decay time of the correlation coefficient in the presence of zinc (see Figure S5B, blue curve). This indicates that zinc induces the formation of large particles in solution. The control experiments without zinc showed no increase in turbidimetry upon heating (Figure 5A, blue dotted curve). Moreover, DLS experiments revealed a size-by-volume peak corresponding to the monomeric state of tau (Figure S5A, blue dotted curve) and a fast decay time in DLS correlogram (Figure S5B, blue dotted curve), confirming that the aggregation observed for tau-WT was zinc-dependent .

When the same experiments were performed with tau-LA (mutant lacking the high affinity R2R3 binding site) no turbidity increase was observed (Figure 5A, brown curves). Moreover, a size-by-volume peak corresponding to the monomeric state of tau (Figure S5A, brown curves) and a late decay time of the DLS correlation function (Figure S5B, brown curves) were observed

both with or without zinc. Thus, absence of zinc binding to the R2R3 region prevented zinc-dependent aggregation of tau.

Turbidimetry experiments with tau-HA (mutant of the N-terminal and C-terminal histidines of tau), showed no increase of the turbidity signal upon heating either (Figure 5A, oranges curves). In addition, zinc did not trigger the formation of tau polymers as shown in volume size distribution (Figure S5A, orange curves) or late decay time of the DLS correlogram (Figure S5B, oranges curves), even though this tau-HA mutant binds zinc as shown by our ITC experiments. These findings show that zinc binding to R2R3 is not sufficient to induce the reversible zinc-dependent aggregation of tau and that the reversible aggregation should be triggered by zinc binding to a low affinity site.

To determine which low affinity site plays a major role in zinc induced aggregation, we studied this process using the four single histidine mutants tau-H362A, tau-H374A, tau-H388A, and tau-H407A, in the presence of zinc ions (Figure 5B). While tau-H362A aggregated just as much as WT-tau, tau-H374A exhibits a lower propensity to aggregate, and the two remaining mutants, tau-H388A and tau-H407A, showed a complete absence of aggregation. Thus, perturbation of aggregation upon mutating these amino acids indicates that low affinity binding site in the C-terminal part of tau plays a major role in zinc induced temperature dependent tau aggregation.

Discussion

Despite the clinical importance of tau protein and the recent discovery of zinc ions influencing the aggregation and self-assembly of tau, the number of tau-zinc interaction sites was still under debate [19,20]. In this study we identify 12 zinc-binding amino acids corresponding to three

zinc-binding sites (one in R2R3 region, one in N-terminal and one in C-terminal part). Our findings are consistent with the fact that zinc is mainly tetra-coordinated in proteins by Cys and His amino-acids [28,29]. Among the six amino acids that have been previously suggested to participate in zinc-binding to the R2R3 region of tau [14,16–18], we finally pinpoint the 4 amino acids (H299, C322, H329 and H330) constituting the main zinc-binding site in tau. In addition, we now describe two novel lower affinity zinc binding sites in the C-terminal et N-terminal regions of tau.

Our results show that the zinc binding to tau is sequential and that the low affinity binding sites in the C-terminal et N-terminal regions of tau are independent from one another. Thus, it is likely that the zinc sequential binding scheme involves only two sites - one higher affinity site in the R2R3 region and one additional site, most likely located in the C-terminal region given its proximity to R2R3 repeat. Our findings suggest that the N-terminal region contains the third independent site which does not release any heat upon the binding of zinc, explaining the absence of signal with ITC. Thus, the low affinity parameters determined by our ITC experiments would correspond to zinc binding to the C-terminal site. Favorable entropy ($\Delta S>0$) observed upon zinc binding to the C-terminal region implies formation of hydrophobic contacts. Indeed, mutating this site resulted in the perturbation of tau aggregation in the presence of zinc, as shown by our turbidimetry assays. More precisely, mutation of histidine 388 or 407 to alanine completely abolished zinc-induced aggregation, emphasising the crucial role of these histidines in this process.

To summarize these findings, the following model can be proposed (Figure 6). The first zinc ion binds to the high affinity site (C291, H299, H329 and H330) in the R2R3 region and induces local folding of tau revealing the low-affinity zinc binding site in the C-terminal site (Figure 6A). Further increase in zinc concentration results in zinc binding to both low-affinity sites (Figure

6B), leading to the reversible aggregation of tau (Figure 6C). Decrease in zinc concentration results in disassembly of tau aggregates (Figure 6D).

Our discovery of several zinc binding sites with different affinity points to the fact that zinc concentration in the cellular environment could influence tau function *in vivo* in both healthy and pathological contexts. In AD for example, intraneuronal levels of zinc in cortical cells of patients have been shown to be increased in comparison to healthy cells [30]. Similarly, high concentrations of zinc were found inside the somata and dendrites of AD neurons [31]. This accumulation may be linked to the functionality of zinc-bound proteins, which can be impaired due to alteration of neuronal metabolism in pathology [32–34]. It is possible that the reversible aggregation of tau occurs in neurons as a protective mechanism. Importance of zinc binding to tau has also been evoked in a physiological context, when the zinc concentrations are lower [20]. In healthy neuronal cells, while tau concentration is around 2 μM, zinc is concentrated at nanomolar levels [35]. Even if it is not sufficient to induce the reversible aggregation of tau, zinc could possibly bind to tau through the high-affinity R2R3 site with a 1:1 stoichiometry. This may regulate tau activity by triggering its compaction at specific subcellular structures where tau is known to play a role, such as microtubules or nucleus [2]. Indeed, the high-affinity R2R3 site overlaps with the microtubule-binding site on tau protein [36,37]. Thus, zinc binding to tau may have physiological implications with low-intraneuronal concentrations of zinc, while possibly affecting the pathological aggregation found in tauopathies at high zinc concentration.

Conclusion

In this study, we identify three zinc binding sites of tau protein and provide a model describing sequential binding of zinc ions inducing reversible aggregation of tau. We also found two histidines in the C-terminal binding site that are responsible for zinc-induced aggregation and

that should be investigated for their role in tau pathological aggregation. Overall, the molecular basis of the tau-zinc interaction provided in our study will help understanding the zinc-related tau aggregation processes in both physiological and pathological conditions, thus paving the way for designing potential therapies for tauopathies.

List of abbreviations

AD: Alzheimer's Disease.

PD: Parkinson's Disease.

PHF: Paired Helical Filaments.

ITC: Isothermal Titration Calorimetry.

NMR: Nuclear Magnetic Resonance.

HSQC: Heteronuclear Single Quantum Correlation.

BMRB: Biological Magnetic Resonance Bank.

WT: Wild Type.

HA: High Affinity.

LA: Low Affinity.

DLS: Dynamic Light Scattering.

TCI : Triple Resonance Probe.

TCEP: tris(2-carboxyethyl)phosphine.

Declarations:

Ethic approval and consent to participate

Not applicable.

Consent for publication

Not applicable.

Availability of data and materials

All data generated or analysed during this study and included in this published article (and its supplementary information files).

Competing interests

The authors declare that they have no competing interests.

Funding

This study was partly supported by research funding from the Cancéropôle PACA, Institut National du Cancer and Région Sud.

Authors' contributions

RLR designed and performed most experiments. POT and FD supervised the study. GF performed SPR experiments. AVG performed molecular simulation. FG supervised NMR

experiments and helped with manuscript discussion and writing. SM, DA helped with experiments. PB helped with manuscript discussion. RLR, POT, FD wrote the manuscript.

Acknowledgements

Microcalorimetry, SPR and turbidimetry experiments were performed in Plateforme Interactome NeuroTimone (PINT) of INP, Marseille, France. NMR experiments were conducted in the NMR platform of IMM, Marseille, France. Molecular modelization at shared research facilities of HPC computing resources at Lomonosov Moscow State University.

References

[1] I. Sotiropoulos, M.-C. Galas, J. M. Silva, E. Skoulakis, S. Wegmann, M. B. Maina, D. Blum, C. L. Sayas, E.-M. Mandelkow, E. Mandelkow, M. G. Spillantini, N. Sousa, J. Avila, M. Medina, A. Mudher, L. Buee, *Acta Neuropathol Commun* **2017**, *5*, DOI 10.1186/s40478-017-0489-6.
[2] Y. Wang, E. Mandelkow, *Nat. Rev. Neurosci.* **2016**, *17*, 5–21.
[3] M. Goedert, M. G. Spillantini, *Mol. Brain* **2017**, *10*, 18.
[4] M. Goedert, A. Klug, R. A. Crowther, *J. Alzheimers. Dis.* **2006**, *9*, 195–207.
[5] S. M. Ward, D. S. Himmelstein, J. K. Lancia, L. I. Binder, *Biochem. Soc. Trans.* **2012**, *40*, 667–671.
[6] B. Bulic, M. Pickhardt, B. Schmidt, E.-M. Mandelkow, H. Waldmann, E. Mandelkow, *Angew. Chem. Int. Ed Engl.* **2009**, *48*, 1740–1752.
[7] A. Ochalek, B. Mihalik, H. X. Avci, A. Chandrasekaran, A. Téglási, I. Bock, M. L. Giudice, Z. Táncos, K. Molnár, L. László, J. E. Nielsen, B. Holst, K. Freude, P. Hyttel, J. Kobolák, A. Dinnyés, *Alzheimers. Res. Ther.* **2017**, *9*, 90.
[8] Z. Xie, H. Wu, J. Zhao, *Neurotoxicology* **2020**, *80*, DOI 10.1016/j.neuro.2020.07.003.
[9] W. P. Esler, E. R. Stimson, J. M. Jennings, J. R. Ghilardi, P. W. Mantyh, J. E. Maggio, *J. Neurochem.* **1996**, *66*, 723–732.
[10] S. Ayala, P. Genevaux, C. Hureau, P. Faller, *ACS Chem. Neurosci.* **2019**, *10*, DOI 10.1021/acschemneuro.9b00239.
[11] A. D. Efimova, R. K. Ovchinnikov, A. Y. Roman, A. V. Maltsev, V. V. Grigoriev, E. A. Kovrazhkina, V. I. Skvortsova, *Mol. Biol. (Mosk.)* **2017**, *51*, 387–399.
[12] A. Caragounis, K. A. Price, C. P. W. Soon, G. Filiz, C. L. Masters, Q.-X. Li, P. J. Crouch, A. R. White, *Free Radic. Biol. Med.* **2010**, *48*, 1152–1161.
[13] C. Garnier, F. Devred, D. Byrne, R. Puppo, A. Y. Roman, S. Malesinski, A. V. Golovin, R. Lebrun, N. N. Ninkina, P. O. Tsvetkov, *Sci. Rep.* **2017**, *7*, 1–10.
[14] Z.-Y. Mo, Y.-Z. Zhu, H.-L. Zhu, J.-B. Fan, J. Chen, Y. Liang, *J. Biol. Chem.* **2009**, *284*, 34648–34657.
[15] Y. Huang, Z. Wu, Y. Cao, M. Lang, B. Lu, B. Zhou, *Cell Rep.* **2014**, *8*, 831–842.

[16] J.-Y. Hu, D.-L. Zhang, X.-L. Liu, X.-S. Li, X.-Q. Cheng, J. Chen, H.-N. Du, Y. Liang, *Biochim. Biophys. Acta* **2017**, *1863*, 414–427.
[17] X. Li, X. Du, J. Ni, *Int. J. Mol. Sci.* **2019**, *20*, DOI 10.3390/ijms20030487.
[18] A. C. Jiji, A. Arshad, S. R. Dhanya, P. S. Shabana, C. K. Mehjubin, V. Vijayan, *Chemistry – A European Journal* **2017**, *23*, 16976–16979.
[19] G. G. Moreira, J. S. Cristóvão, V. M. Torres, A. P. Carapeto, M. S. Rodrigues, I. Landrieu, C. Cordeiro, C. M. Gomes, *Int. J. Mol. Sci.* **2019**, *20*, 5979.
[20] A. Y. Roman, F. Devred, D. Byrne, R. La Rocca, N. N. Ninkina, V. Peyrot, P. O. Tsvetkov, *J. Mol. Biol.* **2019**, *431*, 687–695.
[21] Y. Fichou, Y. K. Al-Hilaly, F. Devred, C. Smet-Nocca, P. O. Tsvetkov, J. Verelst, J. Winderickx, N. Geukens, E. Vanmechelen, A. Perrotin, L. Serpell, B. J. Hanseeuw, M. Medina, L. Buée, I. Landrieu, *Acta Neuropathol Commun* **2019**, *7*, 31.
[22] S. Wegmann, B. Eftekharzadeh, K. Tepper, K. M. Zoltowska, R. E. Bennett, S. Dujardin, P. R. Laskowski, D. MacKenzie, T. Kamath, C. Commins, C. Vanderburg, A. D. Roe, Z. Fan, A. M. Molliex, A. Hernandez-Vega, D. Muller, A. A. Hyman, E. Mandelkow, J. P. Taylor, B. T. Hyman, *EMBO J.* **2018**, *37*, DOI 10.15252/embj.201798049.
[23] V. Singh, L. Xu, S. Boyko, K. Surewicz, W. K. Surewicz, *J. Biol. Chem.* **2020**, DOI 10.1074/jbc.AC120.013166.
[24] A. Savastano, D. Flores, H. Kadavath, J. Biernat, E. Mandelkow, M. Zweckstetter, *Angew. Chem. Int. Ed Engl.* **2021**, *60*, 726–730.
[25] P. Barré, D. Eliezer, *Protein Sci.* **2013**, *22*, 1037–1048.
[26] C. Wang, R. Vernon, O. Lange, M. Tyka, D. Baker, *Protein Sci.* **2010**, *19*, 494–506.
[27] S. Bibow, M. D. Mukrasch, S. Chinnathambi, J. Biernat, C. Griesinger, E. Mandelkow, M. Zweckstetter, *Angew. Chem. Int. Ed Engl.* **2011**, *50*, 11520–11524.
[28] S. F. Sousa, A. B. Lopes, P. A. Fernandes, M. J. Ramos, *Dalton Trans.* **2009**, 7946–7956.
[29] M. Laitaoja, J. Valjakka, J. Jänis, *Inorg. Chem.* **2013**, *52*, 10983–10991.
[30] D. Religa, D. Strozyk, R. A. Cherny, I. Volitakis, V. Haroutunian, B. Winblad, J. Naslund, A. I. Bush, *Neurology* **2006**, *67*, 69–75.
[31] S. W. Suh, K. B. Jensen, M. S. Jensen, D. S. Silva, P. J. Kesslak, G. Danscher, C. J. Frederickson, *Brain Res.* **2000**, *852*, 274–278.
[32] J. L. Smith, S. Xiong, M. A. Lovell, *Neurotoxicology* **2006**, *27*, 1–5.
[33] S. L. Sensi, P. Paoletti, A. I. Bush, I. Sekler, *Nat. Rev. Neurosci.* **2009**, *10*, 780–791.
[34] T. Po, R. Ay, B. Ve, N. Aa, S. Mp, V. Vi, B. Mf, Z. Dv, Z. A. A. Jr, D. F, G. Av, P. Se, Z. Ey, *Front. Mol. Neurosci.* **2018**, *11*, 459–459.
[35] J. H. Weiss, S. L. Sensi, J. Y. Koh, *Trends Pharmacol. Sci.* **2000**, *21*, 395–401.
[36] G. Lee, R. L. Neve, K. S. Kosik, *Neuron* **1989**, *2*, 1615–1624.
[37] P. Barbier, O. Zejneli, M. Martinho, A. Lasorsa, V. Belle, C. Smet-Nocca, P. O. Tsvetkov, F. Devred, I. Landrieu, *Front. Aging Neurosci.* **2019**, *11*, DOI 10.3389/fnagi.2019.00204.
[38] M. Margittai, R. Langen, *Proc. Natl. Acad. Sci. U. S. A.* **2004**, *101*, 10278–10283.
[39] M. Margittai, R. Langen, *J. Biol. Chem.* **2006**, *281*, 37820–37827.
[40] X. Chen, M. Chen, N. P. Schafer, P. G. Wolynes, *Proc. Natl. Acad. Sci. U. S. A.* **2020**, *117*, 4125–4130.

	Model	n	K_A (M^{-1})	ΔH (kcal/mol)	ΔS (cal/mol/deg)
tau-WT	Two sets of sites	3*	$2.1\pm0.7\times10^6$ $5.0\pm1.6\times10^4$	-1.1±0.2 -2.1±0.2	-6.9 14.1
	Sequential binding sites	2*	$1.3\pm0.2\times10^6$ $2.7\pm0.3\times10^4$	-9.6±0.1 -5.0±0.2	-5.7 2.5
tau-HA	One set of site	0.8±0.1	$1.7\pm0.2\times10^5$	-7.4±0.3	-2.3
tau-LA	-	-	-	-	-

Table 1: Binding models and corresponding thermodynamic parameters for ITC experiments of tau and tau constructs. * For tau-WT, stoichiometries (n) were fixed, while others were determined by fitting. Tau-LA titration did not release any heat.

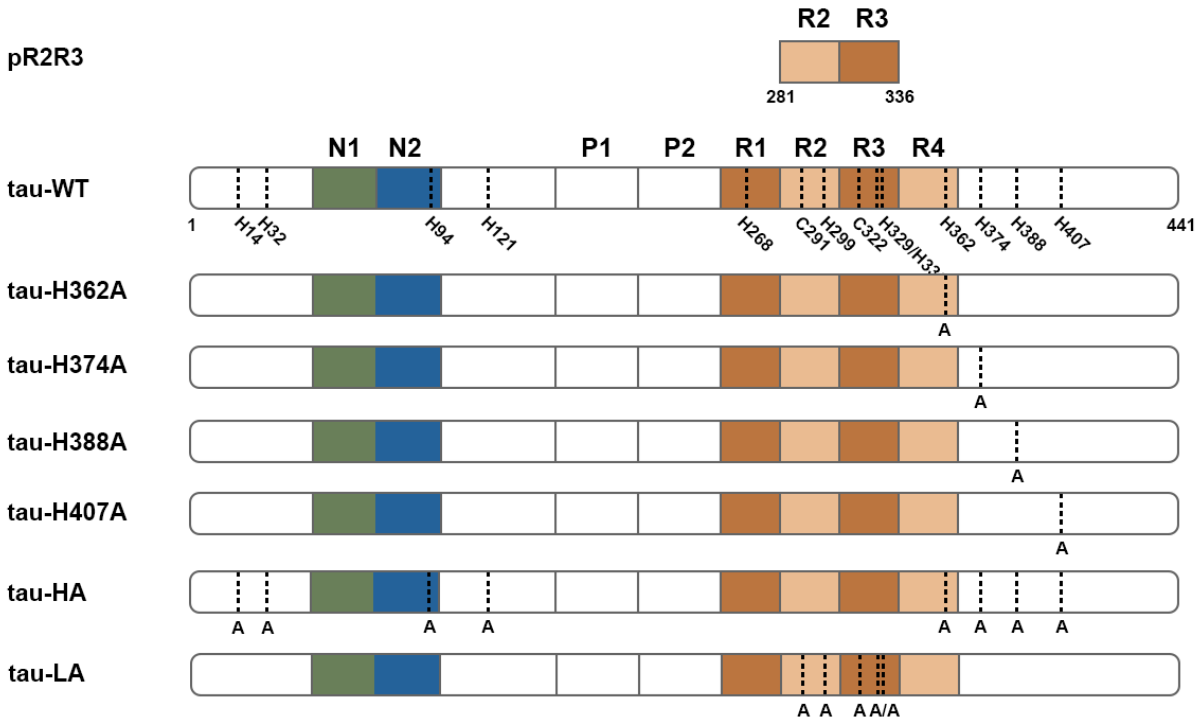

Figure 1 : pR2R3 peptide and tau sequences of mutants (HA : High Affinity ; LA : Low Affinity). Cysteines and histidines are represented on the tau-WT sequence, and alanines mutations for each mutant are shown below histidines and cysteines positions.

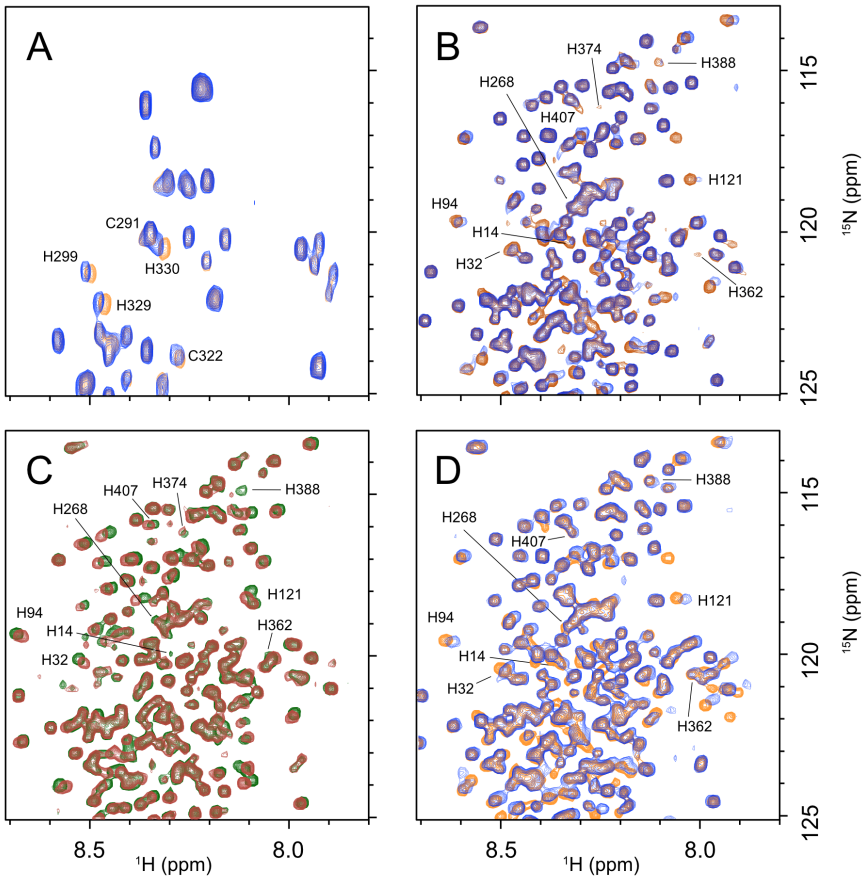

Figure 2: ^{15}N HSQC spectra of tau constructs. A: ^{15}N HSQC spectrum of 1 mM unlabeled pR2R3 at natural abundance in the absence (orange peaks) or in the presence of 3 mM zinc (blue peaks). B: ^{15}N HSQC spectrum of 50 μM ^{15}N-labeled tau-WT in the absence (orange peaks) or in the presence of 300 μM zinc (blue peaks). C: ^{15}N HSQC spectrum of 50 μM ^{15}N-labeled tau-WT at pH 6.1 (green peaks) and 6.7 (red peaks). D: ^{15}N HSQC spectrum of tau-H374A in the absence (orange peaks) or in the presence of zinc (blue peaks). All the experiments were done at 7°C to avoid aggregation in 20 mM MES 100 mM NaCl pH 6.5 unless otherwise stated.

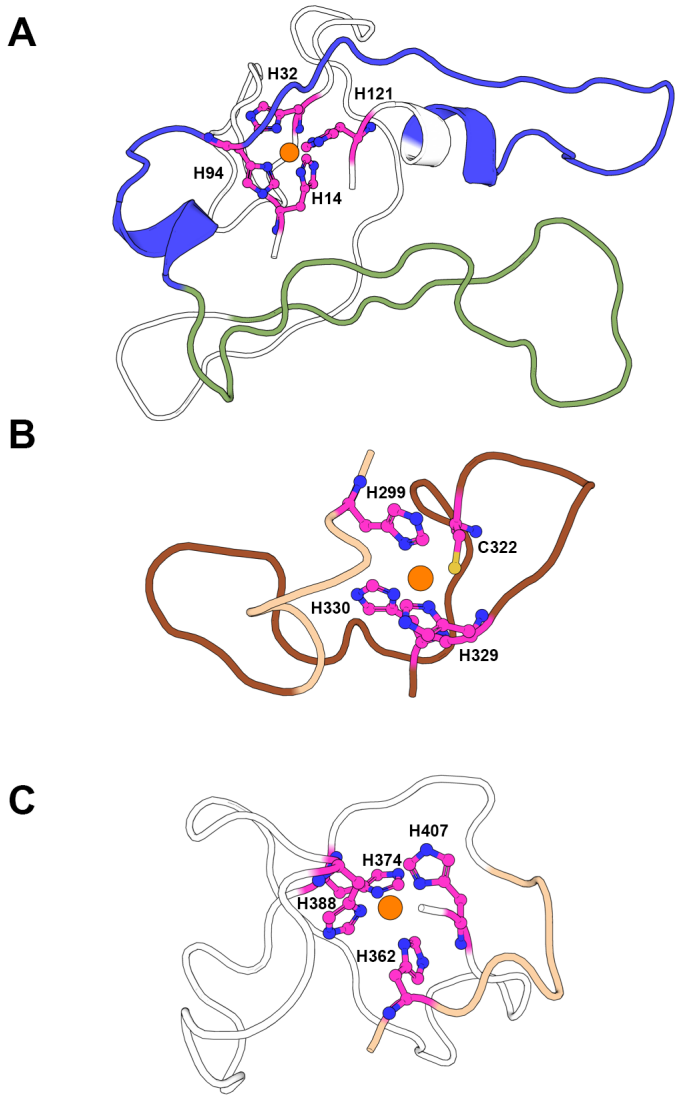

Figure 3: 3D models of the zinc-binding sites on tau. A: N-terminal (13-122), B: R2R3 (298-331) and C: C-terminal (361-408) regions of tau in the presence of zinc (orange sphere).

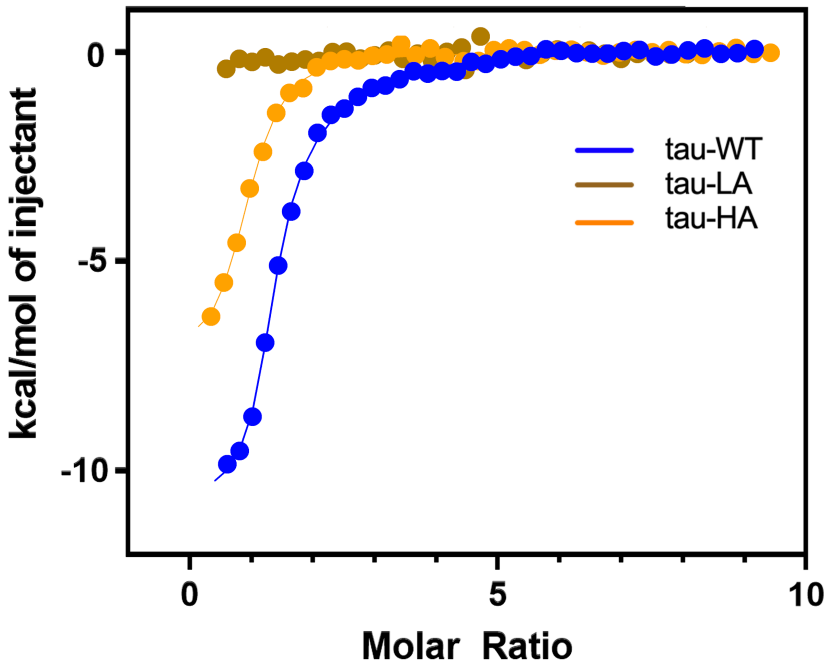

Figure 4: ITC curves of tau-zinc interactions. 50 µM of tau-WT (blue), tau-HA (orange), and tau-LA (brown) were titrated by zinc at 10°C in Tris 50 mM TCEP 1 mM pH 7.5 buffer. Data were fitted with corresponding models (Table 1) except for tau-LA, where zinc did not interact. For tau-WT, the fitting shown here corresponds to a sequential model with 2 sites.

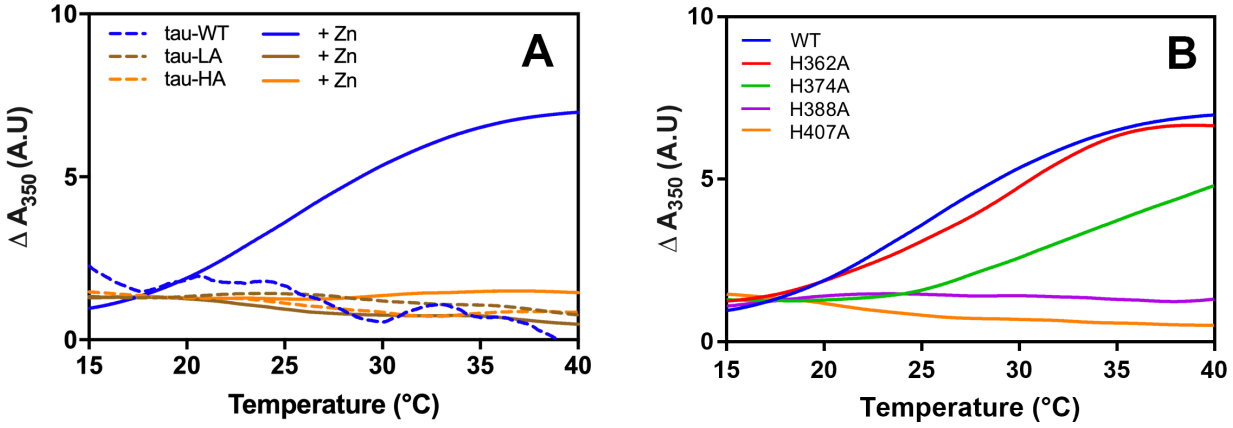

Figure 5: Turbidity assays of tau mutants in the presence of zinc. A: Turbidity assays of 30 μM of tau-WT, tau-LA and tau-HA in the absence (dotted lines) and in the presence (solid lines) of 120 μM of zinc. B: Turbidity assays of 30 μM of tau-WT, tau-H362A, tau-H374A, tau-H388A, tau-H407A in the presence of 120 μM of zinc. All the samples were heated from 15°C to 40°C while measuring the turbidity at 350 nm.

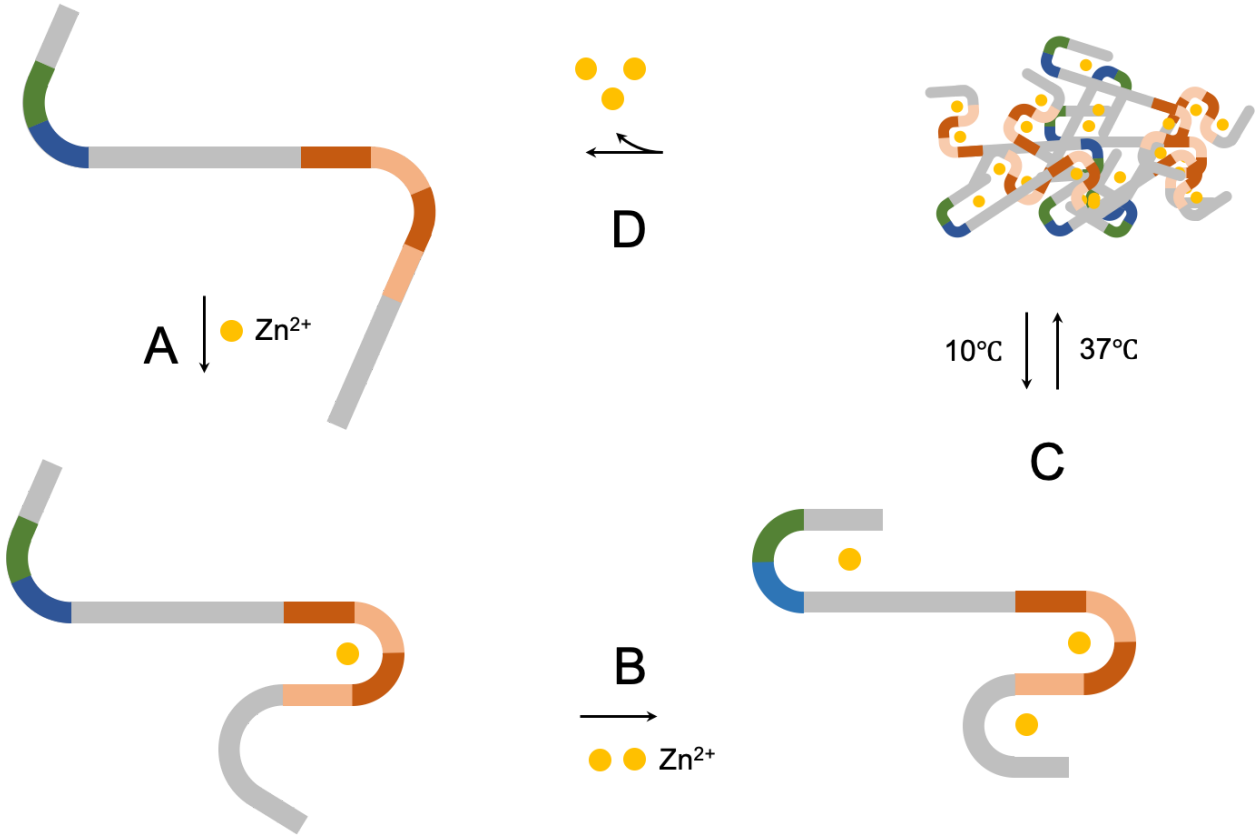

Figure 6. The schematic representation of sequential zinc binding to tau. A : in the presence of limited amount of zinc it binds to the high affinity R2R3 binding site, which then induces the formation of the low affinity C-terminal binding site B : in the presence of higher concentration of zinc, both N-terminal and C-terminal low affinity sites bind zinc. C : increasing temperature to 37°C induces the formation of amorphous aggregates. Steps B and C can be separated *in vitro* by performing step B at low temperature, but *in vivo* at 37°C those two steps would be simultaneous thus indistinguishable. D : removing zinc induces the disassembly of the aggregate.